RSC Advances




ROYAL SOCIETY OF CHEMISTRY

www.rsc.org/advances

## Graphic Abstract

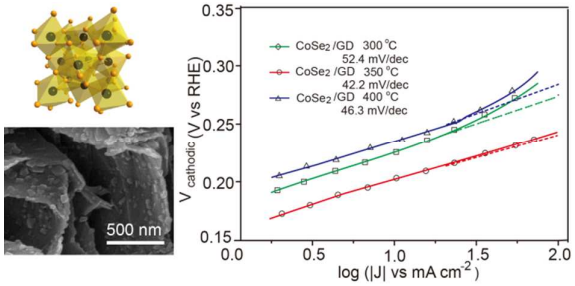


We report one-step synthesis of cubic pyrite-type $CoSe_2$ electrocatalyst toward hydrogen evolution reaction, exhibiting a Tafel slope of ~40 mA/decade.

RSC Advances

RSC Publishing

COMMUNICATION

# One-step synthesis of cubic pyrite-type $CoSe_2$ at low temperature for efficient hydrogen evolution reaction

Cite this: DOI: 10.1039/x0xx00000x

Hongxiu Zhang, Lecheng Lei, Xingwang Zhang*

Received 00th July 2014,
Accepted 00th July 2014

DOI: 10.1039/x0xx00000x

www.rsc.org



**Cubic pyrite-type $CoSe_2$ was synthesized by a one-step method, *via* the reaction between drop casted $CoCl_2$ and Se vapour. The as-grown $CoSe_2$ nanoparticles exhibited high activity toward hydrogen evolution reaction with a low Tafel slope of ~40 mV decade$^{-1}$, accompanied by a large current density and excellent durability.**

Tremendous efforts have been being devoted to the efficient generation of hydrogen through electrolysis or photoelectrochemical reaction.[1-9] Platinum is the most famous catalyst for the hydrogen evolution reaction (HER), however, the large scale application of Pt has been limited by its high cost and low abundance, so developing HER catalysts based on cheap and earth abundant elements has been actively pursued.[10-16] Recently, the transition metal dichalcogenides ($MX_2$, where typically M = Mo, W, Fe, Co, or Ni and X = S or Se) have received considerable attention as cheap and earth abundant catalysts for HER.[17-22] Among these electrocatalysts, cubic pyrite-structure $MX_2$, without needing any special modification or treatment, has shown the high intrinsic activity and excellent durability toward the HER possibly attributed to the unique crystal structure, where the metal atoms are octahedrally bonded to adjacent chalcogen atoms.[17,20 ,23-26] Cubic pyrite-structure $CoSe_2$, exhibited the best HER activity among that of $MX_2$ with a Tafel slope of ~40 mV decade$^{-1}$.[17, 20]

$CoSe_2$, as a well-known oxygen reduction reaction catalyst, has been synthesized by hydrothermal synthesis method.[27-30] It is noteworthy that cubic pyrite-type[27, 28]and orthorhombic marcasite-type $CoSe_2$[29, 30]under the similar reaction conditions have been both reported, and there is seldom document about the manipulation of the crystal structure of $CoSe_2$ in the hydrothermal process. In fact, these two phases have the similarity structural and the small lattice mismatch resulting in the easy epitaxial growth between them,[31] so it is very challenging to prepare the preferred cubic pyrite-type $CoSe_2$ in the hydrothermal process. Recently, Kong et al [17] reported that cubic pyrite-type $CoSe_2$ nanoparticles were synthesized by converting e-beam evaporated Co thin films through a selenization reaction at 500 ℃. Recently, Kong et al further reported a two-step process to synthesize pyrite-type $CoSe_2$ on carbon fiber paper, with a small fraction of marcasite-structure $CoSe_2$, through reacting Se with cobalt oxide, which was prepared from the pyrolysis of cobalt (II) nitrate (500 ℃).[20] Faber et al synthesized pyrite-type $CoS_2$, the $CoSe_2$ analog, through the sulfidation of cobalt hydroxide carbonate hydrate at 500 ℃.[24] Moreover, as we know[12, 32, 33], for large-scale applications in hydrogen energy, HER catalysts should be prepared in scalable processes that are much less energy intensive and costly. Thus, it is desirable to explore easy and scalable approach for the synthesis of cubic pyrite-type $CoSe_2$.

In this letter, for the first time, we reported one step synthesis of pure cubic pyrite-type $CoSe_2$, i.e. polycrystalline trogtalite, by reacting drop casted amorphous $CoCl_2$ coating with Se vapour. We would like to highlight that this method is facile, environmental friendly (use ethanol as solvent), and scalable. The microscopic and structural characterizations were comprehensively conducted. The electrocatalytic activity toward HER of pyrite-type $CoSe_2$ was in investigated.

Typically, the $CoSe_2$ nanoparticles on graphite disks (GD) were synthesized through a new reaction, i.e. reacting Se vapour with $CoCl_2$ at low temperature of 350 ℃ as shown in Fig. 1A. The experimental methods are discussed in detail in the Supporting Information. Briefly, $CoCl_2$•$6H_2O$ was coated on the graphite through the drop casting method using ethanol as solvent as illustrated in Fig. 1A, and a typical loading of $CoSe_2$ on graphite was 2.8 mg cm$^{-2}$. Note that $CoCl_2$•$6H_2O$ is stable to air and water, moreover, it can be soluble in many solvents. The GD substrate covered with $CoCl_2$•$6H_2O$ was located in a home-built tube reactor. When the temperature increased to 350 ℃, $H_2O$ in $CoCl_2$•$6H_2O$ would be vaporized as confirmed in Fig. S1A (ESI†), Then the reaction between $CoCl_2$ and Se vapour was achieved to form $CoSe_2$ at 350 ℃. The reaction is[18]:

$$CoCl_2\ (s) + 2Se\ (g) \rightarrow CoSe_2\ (s) + Cl_2\ (g) \qquad (1)$$

This reaction is possibly thermodynamically favourable because crystal $CoSe_2$ is very stable at high temperature, and the reaction generates gaseous products further driving the equilibrium to the right-hand side. Moreover, $CoCl_2$ was amorphous, as confirmed in Figure. S1B (ESI†), which would decrease the energy of the reaction needed. Thus, the reason of easy and low-temperature formation of cubic pyrite-type $CoSe_2$ might be attributed to the thermodynamically favourable reaction between amorphous $CoCl_2$ and Se vapour.

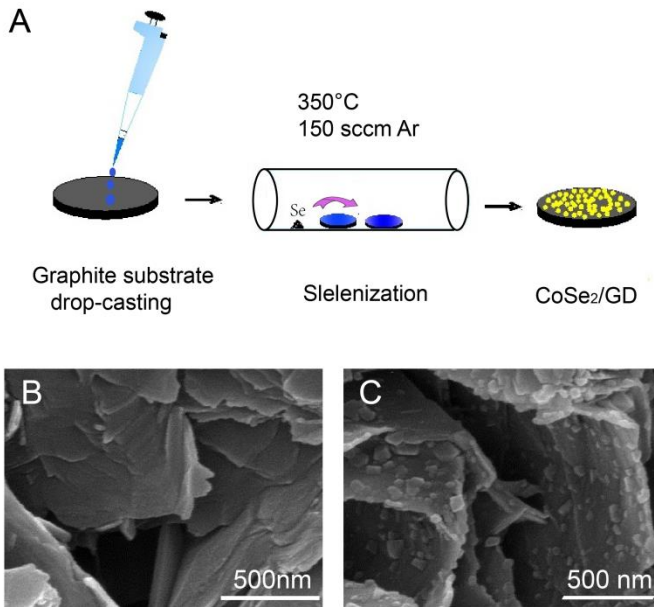


Fig. 1 Synthesis of $CoSe_2$ on GD. (A) Schematic illustration of synthesis of $CoSe_2$/GD through reacting $CoCl_2$ with Se vapour. (B) A representative SEM image of the original GD. (C) A typical SEM image of $CoSe_2$/GD synthesized at 350 ℃ showing that the surface of GD was covered by $CoSe_2$ particles.

First, we investigated the morphology of $CoSe_2$ samples grown at 350 ℃ by SEM as shown in Fig. 1C. It was seen that the particle size of $CoSe_2$ on GD was about 50-100 nm and uniform. It was interestingly observed that the morphology of $CoSe_2$ particles was strongly influenced by the synthesis temperature. $CoSe_2$ particles synthesized at 300 ℃ were hard to observe because of the aggregation of $CoSe_2$ particles as shown in Fig. S2A (ESI†). $CoSe_2$ synthesized at 400 ℃ were composed of large particles (>500 nm) as shown in Fig. S2B (ESI†).

The phase identity of $CoSe_2$/GD products was determined using powder X-ray diffraction (XRD) as shown in Fig. 2A. A broad diffraction peak appeared at $2\theta \approx 26.28^{o}$, and $2\theta \approx 42.64 \sim 44.60^{o}$ mainly corresponding to graphite 2H (ICDD PDF 75-1621) contributed from the graphite disk support. According to the ICDD PDF 88-1712 (No. 205) card, the XRD pattern showed an excellent agreement with the main peaks of the standard spectrum diagram. The XRD patterns show four peaks located at $2\theta \approx$ 30.5, 34.3, 37.6 and 51.8 $^{o}$, which correspond to the (2 0 0), (2 1 0), (2 1 1) and (3 1 1) planes of cubic pyrite-type $CoSe_2$, i.e. trogtalite, respectively. Thus, the peaks of $CoSe_2$ products can be indexed to pyrite-type $CoSe_2$ (space group: Pa3, a=5.87 Å). The marcasite-type $CoSe_2$ (space group Pmnn, a=3.60 Å, b=4.84 Å, c=5.72 Å) was not detected in the PXRD pattern. In order to further confirm the crystal structure of the as-synthesised $CoSe_2$, transmission electron microscopy (TEM) was used to characterize it as shown in Fig. 2B. The TEM image shows a clear crystal lattice, which reveals the resolved lattice fringes of $CoSe_2$ (211) plans with a spacing of 2.39 Å as shown in Fig. 2B. Moreover, as shown in Fig. 2B (inset), the fast Fourier transform (FFT) image further reveals the $CoSe_2$ herein is the cubic pyrite-type phase. It was noteworthy that the crystal structure of $CoSe_2$ synthesized at 500 ℃ was also pyrite-type $CoSe_2$ as shown in Fig. S 5(ESI†). Raman spectrum of the as-obtained $CoSe_2$ on GD was shown in Fig. 2C. The sharp peak at 173 $cm^{-1}$ was assigned to the Se–Se stretching mode of cubic $CoSe_2$;[34] the peak at 187 $cm^{-1}$ is associated with cubic $CoSe_2$;[35] the broad peak at 250 $cm^{-1}$ should be attributed to the tiny amorphous Se.[20, 36, 37] These results further verified the composition and structure of the as-grown $CoSe_2$ on GD. It was well-documented that the activity of HER catalyst was expected to be sensitive to the valence state and coordination environment of the metal centre. So, we revealed the electron-binding energies of Co and Se in cubic pyrite-type $CoSe_2$ as shown in Fig. 2D and E. It was seen that the binding energies of Co $2p_{3/2}$ and Co $2p_{1/2}$ were observed corresponding to 778.4 eV and 793.7eV, respectively.[20,38-41] Se $3d_{5/2}$ and Se $3d_{3/2}$ located at 54.6 and 55.3 eV, indicating the oxidation state of -2 for Se.[42, 43] In contrast, the binding energies of Co $2p_{3/2}$ and Co $2p_{1/2}$ of elemental Co are 778.5 eV[44] and 793.3 eV,[45] respectively. For elemental Se, the binding energy of Se $3d_{5/2}$ is 55.5 eV.[46] Thus, these results illustrated the formation of cubic pyrite-type $CoSe_2$ through the reaction of $CoCl_2$ and Se vapour.

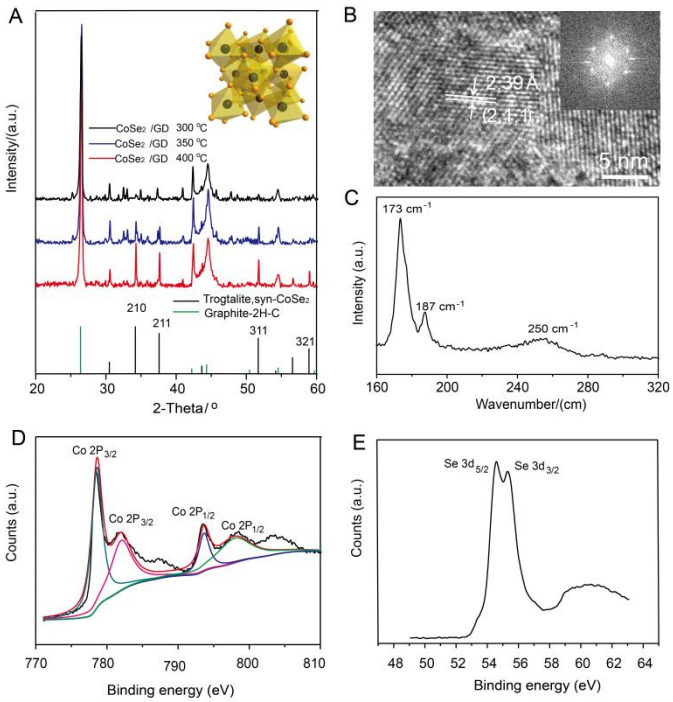


Fig. 2 Structural characterizations of $CoSe_2$ in $CoSe_2$/GD. (A) XRD patterns of $CoSe_2$/GD synthesized at different temperatures and schematic crystal structure of cubic pyrite-type $CoSe_2$ (inset). (B) High-resolution TEM image and a typical fast Fourier transform (FFT) image of an as-grown $CoSe_2$ (inset). (C) Raman spectra of $CoSe_2$/GD. (D) and (E) were XPS spectra of Co 2p region and Se 3d region, respectively.

The electrocatalytic activities of various $CoSe_2$/GD samples were evaluated with a three-electrode electrochemical cell in 0.5 M $H_2SO_4$ solution purged with $H_2$(g) (experimental details in the ESI†). We investigated the effect of the amount of $CoSe_2$ loadings (0.01-4.0 mg $cm^{-2}$) in $CoSe_2$/GD on the HER performances as shown in Fig. S6 (ESI†). It was observed that the best $CoSe_2$ loading on GD toward



 

HER was 2.8 mg $cm^{-2}$. We comprehensively investigated the effect of reaction temperature of $CoSe_2$/GD samples with a $CoSe_2$ loading of 2.8 mg $cm^{-2}$ on their HER performances. Polarization curves after *i*R corrected showing the geometric current density (*J*) plotted against the applied potential of $CoSe_2$/GD samples synthesized at different temperatures were exhibited in Fig. 3A and B. As expected, the bare GD electrode was totally inactive towards HER. It was interesting to observe the high current densities ($J_{cathodic}$> 200 mA $cm^{-2}$) under low applied overpotentials on all samples. Moreover, the reaction temperature had a strong influence on the HER performance of $CoSe_2$/GD, and $CoSe_2$/GD sample synthesized at 350 ℃ exhibited the best HER activity. The superior HER activities of $CoSe_2$ synthesised at 350 ℃ were further illustrated by comparing their Tafel slopes as shown in Fig. 3C. It was seen that the Tafel slopes of samples grown at 300, 350, and 400 ℃ were 52.4, 42.2, and 46.3 mV $decade^{-1}$, respectively, showing the same trend as above.

Three possible reaction steps have been suggested for the HER in acidic media, commonly named the Volmer (eq (2)), Heyrovsky (eq (3)), and Tafel reactions (eq (4)).[47]

$$H_3O^+ + e^- \rightarrow H_{ads} + H_2O \quad (2)$$

$$H_{ads} + H_3O^+ + e^- \rightarrow H_2 + H_2O \quad (3)$$

$$H_{ads} + H_{ads} \rightarrow H_2 \quad (4)$$

When the Volmer reaction is the rate-determining step of the HER, a slope of ~120 mV $decade^{-1}$ should be observed. Whereas if Heyrovsky or Tafel reactions is the rate-limiting step, Tafel slopes of ~30 and ~40 mV $decade^{-1}$ can be obtained, respectively.[48] In this study, the observed Tafel slope of 42.2 mV $decade^{-1}$ indicated that the Volmer-Heyrovsky HER mechanism (eq (2) and (3)) is operative in the HER catalyzed by $CoSe_2$/GD.[13] Five experiments were performed to verify the data accuracy, the Tafel slopes were 43.3, 42.6, 42.7, 42.2, 42.2 mV $decade^{-1}$, respectively, and the corresponding standard deviation was 0.45. It is well known that the Tafel slope is considered as an inherent property of the HER catalyst, so the small Tafel slope of ~40 mV $decade^{-1}$ in this study is expected to be more beneficial for practical applications, because it can provide a remarkably increased HER rate with the moderate increase of applied overpotential.

Additionally, electrochemical impedance spectroscopy (EIS) was used to investigate the kinetics on $CoSe_2$ under the catalytic HER operating conditions as shown in Fig. 3D. The charge transfer resistance ($R_{ct}$) associated with $H_2$ (g) evolution for each electrode was extracted by modelling the EIS data using a simplified Randles equivalent circuit (ESI†). $R_{ct}$ for $CoSe_2$/GD grown at 300, 350 and 400 °C were 3.6, 8.8, 16.2 Ω, respectively. The EIS data confirmed that the superior activity $CoSe_2$/GD grown at 350 ℃ was possibly attributed to the facile kinetics toward $H_2$ (g) evolution. We also measured the capacitive current for $CoSe_2$/GD samples grown at 300 (Fig. S7A(ESI†)), 350 (Fig. 3E), and 400 ℃ (Fig. S7B(ESI†)) as a function of scan rate to extract the double layer capacitance ($C_{dl}$) of each electrode, which serves as an estimate of the effective electrochemically active surface area of the solid–liquid interface. The $C_{dl}$ of $CoSe_2$/GD grown at 300, 350, and 400 ℃ is 3.4, 5.5 and 4.5 mF $cm^{-2}$, respectively. Even though these $C_{dl}$ values exhibited differences, it was unlikely that such a small variation in $C_{dl}$ accounted for the obvious differences in observed performance (Figure 3A and B), although the morphologies of $CoSe_2$/GD grown at 300 (Fig. S2A (ESI†)), 350 (Fig. 1B), and 400 ℃ (Fig. S2B (EIS†)) were different. Consequently, the differences of HER performance of $CoSe_2$/GD grown at 300, 350, and 400 ℃ were mainly ascribed to the different intrinsic activity, i.e. the different kinetics toward $H_2$ evolution.

Furthermore, besides the electrocatalytic activity, it is well-established that the stability is also a crucial factor to develop HER catalyst. To evaluate the stability, long term durability of $CoSe_2$/GD grown at 350 ℃ was assessed by a 24 h stable current measurement as shown in Fig. 3F. It was seen that over the duration of the 24 h stability measurement, the cathodic overpotential required to maintain $J_{cathodic}$ = 10 mA $cm^{-2}$ was inherently stable, which just increased only about 30 mV. It should be noted that the increasing of cathodic overpotential to maintain $J_{cathodic}$ = 10 mA $cm^{-2}$ mainly occurred at the beginning of the stability test (0-12 h); from 12 h to 24 h, the cathodic overpotential to maintain $J_{cathodic}$ = 10 mA $cm^{-2}$ slightly increased only by 3 mV.

Lastly, we attempt to compare the performance of our $CoSe_2$/GD with that synthesized by two-step process.[20] $CoSe_2$/GD grown at 350 ℃ exhibited pretty low onset overpotential of -135 mV. Generally, the onset overpotential depends on several factors, such as catalyst loading amount, intrinsic activity, and purity. Considering the similar intrinsic activity of samples by one-step and two-step (a Tafel slope of ~40 mV/dec), the lower onset overpotential in this study was possibly attributed to the high-purity crystal phase of pyrite-type $CoSe_2$ and higher loading of $CoSe_2$. Moreover, it required a applied overpotential of -193 mV to obtain the significant $H_2$(g) evolution ($J_{cathodic}$ = 10 mA $cm^{-2}$). These values were similar to that of $CoSe_2$ converted form CoO on carbon paper.[20] Thus, it was concluded that our simple method can produce $CoSe_2$ catalysts with competitive HER performance.

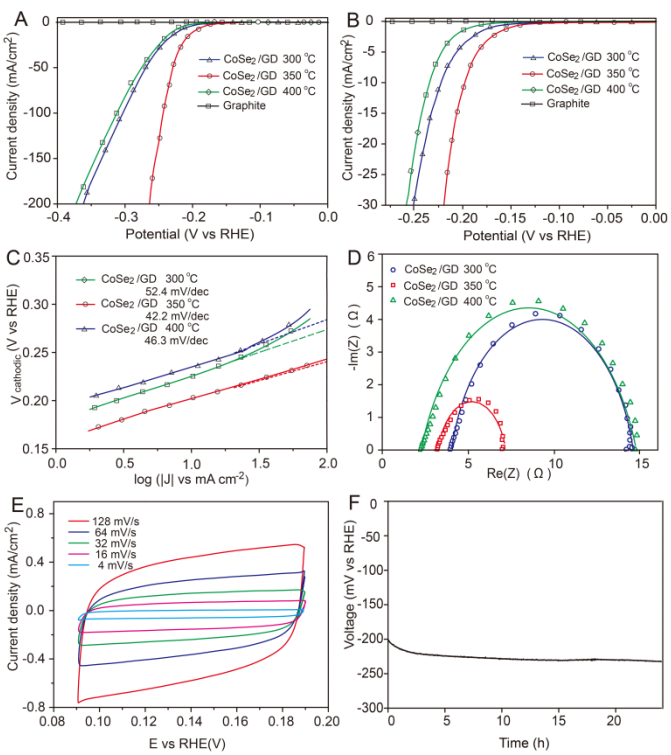


Fig. 3 Electrocatalytic performance toward HER of $CoSe_2$/GD samples by different temperatures. Polarization curves at (A) higher and (B) lower applied potentials. (C) Tafel analysis of the data presented in A and B. (D) Nyquist plots showing the electrode kinetics of samples. (E) Cyclic voltammograms recorded for a $CoSe_2$/GD electrode at various scan rates to determine the double layer capacitance ($C_{dl}$). (F) Long-term stability measurement for a representative $CoSe_2$/GD sample at 350 ℃, demonstrating the small

change in the overpotential required to maintain a continuous catalytic current density of $J_{cathodic}$ = 10 mA cm$^{-2}$ for 24 h.

In summary, we reported a one-step method to synthesize pure cubic pyrite-type $CoSe_2$ electrocatalysts toward HER *via* a reaction between drop casted $CoCl_2$ and Se vapour. The structural characterization and electrochemical HER activities of series of $CoSe_2$/GD samples synthesized at different temperatures were systemically investigated. The $CoSe_2$ electrocatalyst on GD showed excellent HER activity with a minimum Tafel slope of ~40 mV decade$^{-1}$. This synthesis approach allows facile preparation of advanced $CoSe_2$ HER electrocatalysts at large scale. This convenient and scalable synthesis method demonstrates a potentially versatile and low-cost strategy to make other transition metal chalcogenides.

This research is supported by NSFC (21276231, 21476201, and U1162128).

## Notes and references

[a] Key Laboratory of Biomass Chemical Engineering of Ministry of Education,

[b] College of Chemical and Biological Engineering, Zhejiang University, Hangzhou, Zhejiang Province 310027, China

[c] E-mail: xwzhang@zju.edu.cn

†Electronic Supplementary Information (ESI) available: Detailed experimental procedures, TGA and SEM images, XRD, EDS, XPS spectra, and other additional graphs. See DOI: 10.1039/c000000x/

1. D. Merki and X. L. Hu, *Energy Environ. Sci.*, 2011, 4, 3878-3888.
2. L. S. Li, Y. H. Yu, F. Meng, Y. Z. Tan, R. J. Hamers and S. Jin, *Nano Lett.*, 2012, 12, 724-731.
3. Y. J. Feng, T. He and N. Alonso-Vante, *Fuel Cells*, 2010, 10, 77-83.
4. W. F. Chen, J. T. Muckerman and E. Fujita, *Chem. Commun.*, 2013, 49, 8896-8909.
5. A. B. Laursen, P. C. K. Vesborg and I. Chorkendorff, *Chem. Commun.*, 2013, 49, 4965-4967.
6. Z. Y. Lu, H. C. Zhang, W. Zhu, X. Y. Yu, Y. Kuang, Z. Chang, X. D. Lei and X. M. Sun, *Chem. Commun.*, 2013, 49, 7516-7518.
7. Y. Xu, R. Wu, J. F. Zhang, Y. M. Shi and B. Zhang, *Chem. Commun.*, 2013, 49, 6656-6658.
8. Y. Yan, B. Y. Xia, X. Y. Qi, H. B. Wang, R. Xu, J. Y. Wang, H. Zhang and X. Wang, *Chem. Commun.*, 2013, 49, 4884-4886.
9. A. B. Laursen, S. Kegnæs, S. Dahl and I. Chorkendorff, *Energy Environ. Sci.*, 2012, 5, 5577-5591.
10. J. R. McKone, S. C. Marinescu, B. S. Brunschwig, J. R. Winkler and H. B. Gray, *Chem. Sci.*, 2014, 5, 865-878.
11. S. P. Berglund, H. C. He, W. D. Chemelewski, H. Celio, A. Dolocan and C. B. Mullins, *J. Am. Chem. Soc.*, 2014, 136, 1535–1544.
12. M. G. Walter, E. L. Warren, J. R. McKone, S. W. Boettcher, Q. Mi, E. A. Santori and N. S. Lewis, *Chem. Rev.*, 2010, 110, 6446–6473.
13. E. J. Popczun, J. R. McKone, C. G. Read, A. J. Biacchi, A. M. Wiltrout, N. S. Lewis and R. E. Schaak, *J. Am. Chem. Soc.*, 2013, 135, 9267-9270.
14. E. J. Popczun, C. G. Read, C. W. Roske, N. S. Lewis and R. E. Schaak, *Angew. Chem. Int. Ed.*, 2014, 53, 5427–5430.
15. Q. Ding, F. Meng, C. R. English, M. Cabán-Acevedo, M. J. Shearer, D. Liang, A. S. Daniel, R. J. Hamers and S. Jin, *J. Am. Chem. Soc.*, 2014, 136, 8504-8507.
16. Q. Liu, J. Tian, W. Cui, P. Jiang, N. Cheng, A. M. Asiri and X. Sun, *Angew. Chem. Int .Ed.*, 2014, 53, 6710-6714.
17. D. S. Kong, J. J. Cha, H. T. Wang, H. R. Lee and Y. Cui, *Energy Environ. Sci.*, 2013, 6, 3553-3558.
18. M. A. Lukowski, A. S. Daniel, F. Meng, A. Forticaux, L. S. Li and S. Jin, *J. Am. Chem. Soc.*, 2013, 135, 10274-10277.
19. J. Bonde, P. G. Moses, T. F. Jaramillo, J. K. Nørskov and I. Chorkendorff, *Faraday Discuss.*, 2008, 140, 219–231.
20. D. Kong, H. Wang, Z. Lu and Y. Cui, *J. Am. Chem. Soc.*, 2014, 136, 4897-4900.
21. M. A. Lukowski, A. S. Daniel, C. R. English, F. Meng, A. Forticaux, R. J. Hamers and S. Jin, *Energy Environ. Sci.*, 2014, 7, 2608-2613.
22. T. F. Jaramillo, K. P. Jorgensen, J. Bonde, J. H. Nielsen, S. Horch and I. Chorkendorff, *Science*, 2007, 317, 100-102.
23. M. Caban-Acevedo, M. S. Faber, Y. Z. Tan, R. J. Hamers and S. Jin, *Nano Lett.*, 2012, 12, 1977-1982.
24. M. S. Faber, R. Dziedzic, M. A. Lukowski, N. S. Kaiser, Q. Ding and S. Jin, *J. Am. Chem. Soc.*, 2014, 136, 10053-10061.
25. A. Ivanovskaya, N. Singh, R. F. Liu, H. Kreutzer, J. Baltrusaitis, T. V. Nguyen, H. Metiu and E. McFarland, *Langmuir*, 2013, 29, 480-492.
26. M. S. Faber, K. Park, M. Cabán-Acevedo, P. K. Santra and S. Jin, *J. Phys. Chem. Lett.*, 2013, 4, 1843-1849.
27. M. R. Gao, X. Cao, Q. Gao, Y. F. Xu, Y. R. Zheng, J. Jiang and S. H. Yu, *ACS Nano*, 2014, 8, 3970-3978.
28. J. L. Yang, X. P. Shen, Z. Y. Ji and G. X. Zhu, *J. Mater. Sci.*, 2013, 48, 7913-7919.
29. Y. J. Feng, T. He and N. Alonso-Vante, *Fuel Cells*, 2010, 10, 77-83.
30. W. X. Zhang, Z. H. Yang, J. W. Liu, Z. H. Hui, W. C. Yu, Y. T. Qian, G. E. Zhou and L. Yang, *Mater. Res. Bull.*, 2000, 35, 2403-2408.
31. R. Sun, M. K. Y. Chan and G. Ceder, *Phys. Rev. B*, 2011, 83, 235311-235322.
32. P. P. Edwards, V. L. Kuznetsov and W. I. David, *Philos. Trans. A Math. Phys. Eng. Sci.*, 2007, 365, 1043-1056.
33. K. Mazloomi and C. Gomes, *Renew. Sust. Energ. Rev.*, 2012, 16, 3024-3033.
34. K. Kodama, R. Jinnouchi, T. Suzuki, T. Hatanaka and Y. Morimoto, *Electrochim. Acta*, 2012, 78, 592-596.
35. L. Zhu, M. Teo, P. C. Wong, K. C. Wong, I. Narita, F. Ernst, K. A. R. Mitchell and S. A. Campbell, *Appl. Catal. A: Gen*, 2010, 386, 157-165.
36. H. Wang, Z. Lu, S. Xu, D. Kong, J. J. Cha, G. Zheng, P. C. Hsu, K. Yan, D. Bradshaw, F. B. Prinz and Y. Cui, *Proc. Natl. Acad. Sci. U. S. A.*, 2013, 110, 19701-19706.
37. V. V. Poborchii, A. V. Kolobov and K. Tanaka, *Appl. Phys. Lett.*, 1998, 72, 1167-1169.
38. W. Huang, Z. Zuo, P. Han, Z. Li and T. Zhao, *J. Electron. Spectrosc. Relat. Phenom.*, 2009, 173, 88-95.
39. M.-R. Gao, S. Liu, J. Jiang, C.-H. Cui, W.-T. Yao and S.-H. Yu, *J. Mater. Chem.*, 2010, 20, 9355-9361.
40. M. C. Biesinger, B. P. Payne, A. P. Grosvenor, L. W. M. Lau, A. R. Gerson and R. S. C. Smart, *Appl. Surf. Sci.*, 2011, 257, 2717-2730.
41. J. Yang, G.-H. Cheng, J.H. Zeng, S.H. Yu, X.M. Liu and Y.-T. Qian, *Chem. Mater.*, 2001, 13, 848-853.
42. Z. Zhang, S. Pang, H. Xu, Z. Yang, X. Zhang, Z. Liu, X. Wang, X. Zhou, S. Dong, X. Chen, L. Gu and G. Cui, *RSC Adv.*, 2013, 3, 16528-16533.
43. N. D. Boscher, C. J. Carmalt and I. P. Parkin, *J. Mater. Chem.*, 2006, 16, 122-127.
44. A. Mandale, S. Badrinarayanan, S. Date and A. Sinha, *J. Electron. Spectrosc. Relat. Phenom.*, 1984, 33, 61-72.
45. J. Bonnelle, J. Grimblot and A. D'huysser, *J. Electron. Spectrosc. Relat. Phenom.*, 1975, 7, 151-162.
46. M. Shenasa, S. Sainkar and D. Lichtman, *J. Electron. Spectrosc. Relat. Phenom.*, 1986, 40, 329-337.
47. B. E. Conway and B. V. Tilak, *Electrochim. Acta*, 2002, 47, 3571-3594.
48. Y. G. Li, H. L. Wang, L. M. Xie, Y. Y. Liang, G. S. Hong and H. J. Dai, *J. Am. Chem. Soc.*, 2011, 133, 7296-7299.



 